Hindawi
Wireless Communications and Mobile Computing
Volume 2022, Article ID 8599257, 11 pages
https://doi.org/10.1155/2022/8599257

Research Article

The Spatial Pattern Strategy of Urban Ecological Patches Based on the Mesoscale WRF-UCM Model: Taking Wuhan City as an Example

Xuesong Li,[1] **Hong Chen**,[2] **and Kai Lin**[1]

[1]*School of Civil Engineering, Architecture and Environment, Hubei University of Technology, Wuhan, Hubei 430068, China*
[2]*School of Architecture & Urban Planning, Huazhong University of Science and Technology, Wuhan, Hubei 430074, China*

Correspondence should be addressed to Xuesong Li; 19890028@hbut.edu.cn

Received 6 June 2022; Revised 8 July 2022; Accepted 12 July 2022; Published 17 August 2022

Academic Editor: Kalidoss Rajakani

In the context of rapid urbanization, the reduction of urban ecological land area, space chaos, and fragmentation have led to a series of climate and environmental problems. This paper takes the ecological patches of the urban climate environment compensation space as the research object and establishes several urban canopy models of several cases based on geographic information data. Then, we input them into the mesoscale WRF-UCM model and simulate after loading the meteorological data to derive the meteorological indicators of each case, quantitatively analyze the meteorological conditions in the ecological patch boundaries with different surface attributes, and conduct research on the "quality-efficiency" correspondence of the physical characteristics of the ecological patches and the spillover effects of climate regulation. Studies have shown that the highest surface temperature difference between water patches and patches with other attributes ΔTsk is up to 6.5°C in winter and 11.5°C in summer. The highest temperature difference at a somatosensory height of 2 meters $\Delta T2$ is up to 2.0°C in winter and 3.0°C in summer, which can improve the surrounding environment. Under light wind conditions, water patches will have a positive spillover effect within 5.5 km of the downwind direction. Based on the data, an optimization strategy for the spatial pattern of urban ecological patches is proposed: the best distribution of water patches that are beneficial to the climate adjustment of Wuhan in winter and summer is in the north or northeast of the city, followed by the south or southwest. The north and northeast of the city should keep the woodland patches and reduce the setting of vegetation/arable land and wetland patches. This research is an interdisciplinary study of urban spatial planning that adapts to climate change, to supplement the deficiencies of urban planning theory, and to provide guidance for the promotion of green and ecological city construction.

1. Introduction

Geography believes that a "city" is a dense combination of people and houses located in an environment with convenient transportation and covering a certain area. The formation of a city is a process in which land use changes and artificial landscapes gradually replace natural landscapes [1]. Land use type refers to the land resource unit with the same land use mode, which is divided according to the regional differences of land use. It is the basic regional unit that reflects the land use, nature, and distribution law. It is a variety of land use categories with different use directions and characteristics formed by human beings in the process of transforming and using land for production and construction. Changes in land use types affect the surface albedo, ground roughness, soil heat exchange, water evapotranspiration, and other characteristics, which have an extremely important impact on climate and land surface processes [2]. The rapid development of cities has changed the land use and reshaped the underlying surface, while changing the balance of radiant energy, reducing the dissipation of heat by air convection, leading to the urban heat island effect and a series of environmental problems [3]. The basic model of landscape structure is patch-corridor-matrix. "Patch" is the basic unit of the landscape pattern, which is different from the surrounding background or the spatial entity of

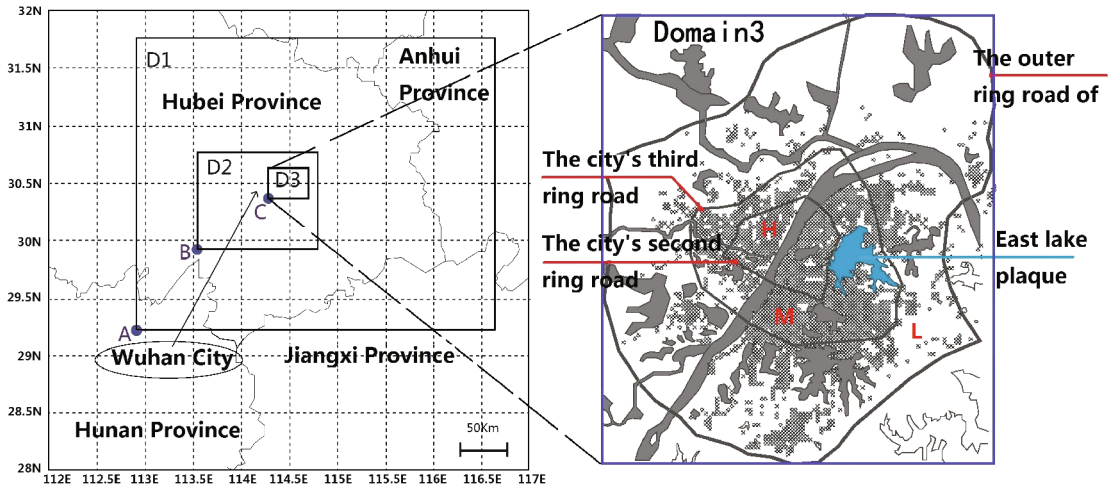

Figure 1: The three-level nesting relationship diagram of the simulation area.

the base (background/matrix), and has relatively homogeneous nonlinear and discontinuous characteristics [4–6]. In tourist areas, patches mainly refer to various consumption places of tourists, such as scenic spots, camping places, and hotels. In terms of tourism landscape resources, it refers to natural landscapes or areas dominated by natural landscapes, such as forests, lakes, and grasslands. Patches are spatial entities with scales, which are different from the surrounding environment (basement) in nature or appearance. Patches can also refer to other small communities scattered in a larger single community, which are caused by natural factors. Urban ecological patch (ecological patch) is a nonlinear, noncontinuous ecological land used in cities to provide ecosystem services and improve regional human-land relationships and relatively homogeneous surface attributes, such as lakes, wetland, woodland, vegetation, and arable land. Types mainly include interference patches, residual patches, environmental resources patches, renewal patches, and introduced patches [7, 8].

Under the action of the atmospheric environment, while the ecological patch itself produces microclimate changes in life activities, the impact on the surrounding climate environment (regulatory effect) is defined as the climate regulation spillover effect. We define the favorable adjustment effect of the climate environment around the ecological patch as a positive spillover effect, such as cooling and ventilation in summer, rising warm current in winter, and humidification of dry islands [9–12]. Conversely, the adverse adjustment effect obtained by the surrounding environment is defined as a negative spillover effect. For example, climate warming produces the "spillover effect" of rising air pollution. Climate change has damaged the health of human life in different ways, including the negative impact on food production, the concentration of thermal stress in materials, the rise of sea level, the increase of storm intensity, the increase of flood and dry weather, and the increase of disease incidence. Climate change indirectly affects people's health through the rise of air pollutant concentration, such as the increase of ozone and fine particles (less than 2 or 5 microns in diameter) on the earth's surface, and sulfate, nitrate, and carbon black dust belong to fine particles. Air pollutants are associated with the rise in the incidence rate of dangerous diseases, including lung cancer and various respiratory diseases, cardiopulmonary diseases, and cardiovascular diseases.

Table 1: Physical process and scheme.

Physical process	Physical scheme
Microphysics	New Thompson solution
Long wave radiation	RRTM scheme
Shortwave radiation	Goddard plan
Near ground floor	MYJ Monin-Obukhov plan
Land surface	Noah land surface model
Planetary boundary	Mellor-Yamada-Janjic plan

As the only physical boundary of the atmosphere, the earth's surface is composed of underlying surfaces with different types of attributes. Its physical characteristics affect the structure of the atmospheric boundary layer and local weather conditions on a dynamic time-space scale [13]. The impact of the underlying surface on the atmosphere is mainly manifested in two aspects: first, the impact on temperature. As temperature is the most important element of climate, it is also the main aspect of the impact of underlying surface on the atmosphere. For the lower atmosphere, because it can hardly absorb solar radiation but can strongly absorb ground radiation, ground radiation has become its main direct heat source. The second is the impact on atmospheric moisture, which also comes from the underlying surface. Under the same meteorological conditions, the surface temperature of different underlying surfaces varies greatly, and the greening of the underlying surface can effectively improve the local microclimate; the local noon solar altitude angle plays a leading role in the surface temperature of the underlying surface. There are many types of ecological patches in the city. Because the absorption, reflection, and evapotranspiration of solar radiation energy are different, the meteorological characteristics are different. Because the unique surface roughness and frictional resistance of

Table 2: Simulation area and grid description.

	Scale (X^*Y^*Z)	Number of grids	Grid size
Domain 1	333*297*20	74*66*35	4.5
Domain 2	154.5*141*20	103*94*35	1.5
Domain 3	60.5*65*20	121*130*35	0.5
Longitude and latitude of center point	30.58°E, 114.31°N		

ecological patches affect energy flow, the difference in heat budget between various types of patches and the substrate will lead to meteorological differences [14, 15]. Only by conducting the "quality-efficiency" correspondence study of climate regulation spillover effects (effects) on ecological patches with various surface attributes (quality) can we truly reveal their internal working methods and operating rules and find the differences in their spillover effects.

2. Materials and Methods

2.1. City Introduction. Wuhan is a national central city in the eastern part of the Jianghan Plain. It has a northern subtropical monsoon (humid) climate, with cold winters and hot summers, with extreme maximum temperatures of 41.3°C and extreme minimum temperatures of -18.1°C [16]. As of the end of 2019, the city area is 8569 km^2, the built-up area is 812.39 km^2, and the permanent population is 11.212 million. Plains account for 81.9%, while low mountains and hills account for 5.8% and 12.3%, respectively. The biggest feature of the surface attribute is the abundant water area of the whole territory, with 166 large and small lakes. The Yangtze River and Han River pass through the city, dividing the city into three towns: Wuchang, Hankou, and Hanyang. Wuhan's wetland resources rank among the top three inland cities in the world, with a natural wetland area of 1561.86 km^2 and an artificial wetland area of 1796.49 km^2, accounting for 39.54% of the city's land area. The rapid development of Wuhan has caused tremendous changes in the city's green space pattern. From 1970 to 2015, the area of arable land decreased by 642.07 km^2. The area of woodland decreased by 11.8 km^2. The water area of East Lake, a national key scenic spot in the main urban area, decreased by 210.26 hectares [17–19]. The expansion of built-up areas, the artificialization of ecological land, and the fragmentation of ecological patches directly affect the urban climate and environment. From the change of landscape index in Wuhan in different periods, the degree of landscape fragmentation has increased in Wuhan on the whole level, and the aggregation and cohesion between patches have declined seriously. Due to the rapid development of urbanization, the landscape index of construction land has changed significantly, gradually from the original dispersion and fragmentation to relative concentration. From the perspective of township level, CONTAG, MESH, and AI in the central region of Wuhan are increasing year by year. It can be seen that the construction land in the central urban area is concentrated, while the patch number (NP), patch density (PD), and Shannon diversity index (SHDI) in the surrounding areas change significantly, which means that the degree of landscape fragmentation in the surrounding areas increases year by year.

2.2. Case Setting. In this study, winter and summer in Wuhan City, which are hot in summer and cold in winter, are selected as the regional meteorological background, and the boundary of the "Donghu water patch" within the main urban area of Wuhan is selected as the target (Figure 1). Within the boundary of the East Lake, five possible land surface types in the city are replaced, five urban canopy models are established, and WRF + UCM simulations are performed. The environmental meteorological indicators of various ecological patches are analyzed, and the differences in the spillover effects of climate regulation are compared. The specific case is described as follows:

Case 1. Maintain the "water patch" of the original water body.

Case 2. Replace the surface attributes in the target area with "vegetation/cultivated land mixed patches."

Case 3. Replace the surface attributes in the target area with "wetland (permanent wetland) patches."

Case 4. Replace the surface attributes in the target area with "woodland (mixed forest) patches."

Case 5. Replace the land surface properties in the target area with construction land, that is, the "no ecological patch case." This case will be used as a reference for other cases.

2.3. Method Introduction and Parameter Setting. This research mainly adopts the mesoscale forecast model (Weather Research and Forecasting (WRF) model) jointly developed by the National Center for Environmental Prediction (NCEP) and the National Center for Atmospheric Research (NCAR). The fifth generation mesoscale model is a mesoscale numerical prediction model jointly developed by the American Center for Atmospheric Research (NCAR) and the University of Pennsylvania (PSU) on the basis of MM4 in recent years. It has been widely used in the study of mesoscale phenomena such as tropical storms, midlatitude cyclone frontal systems, rainstorms, and mesoscale convective systems. It is one of the most widely used mesoscale numerical prediction models in the meteorological field. The version 3.9 we have adopted has integrated single-layer cities, and canopy model (urban canopy model (UCM)) is coupled into the model. On the basis of reflecting the topographic features of the city, it can more accurately

Table 3: Urban canopy parameters.

Urban land intensity	The average height of the building/m	Average roof width/m	Average road width/m	Greening rate %	Artificial heat (w/m^2)	Roof heat capacity ($J\cdot/m^3\cdot K$)	Wall heat capacity ($J\cdot/m^3\cdot K$)	Road heat capacity ($J\cdot/m^3\cdot K$)	Roof thermal conductivity ($J\cdot/m^3\cdot K$)	Wall thermal conductivity ($J\cdot/m\cdot sK$)	Road thermal conductivity ($J\cdot/ms\cdot K$)	Roof absorption rate	Wall absorption rate	Road absorption rate	Reflectivity summer/winter (season)
High	27	55	20	30	160	1.0*106	1.0*106	1.4*106	0.67	0.67	0.4004	0.9	0.9	0.95	0.15/0.18
Medium	21	40	20	35	120	1.0*106	1.0*106	1.4*106	0.67	0.67	0.4004	0.9	0.9	0.95	0.15/0.18
Low	18	25	20	40	100	1.0*106	1.0*106	1.4*106	0.67	0.67	0.4004	0.9	0.9	0.95	0.15/0.18

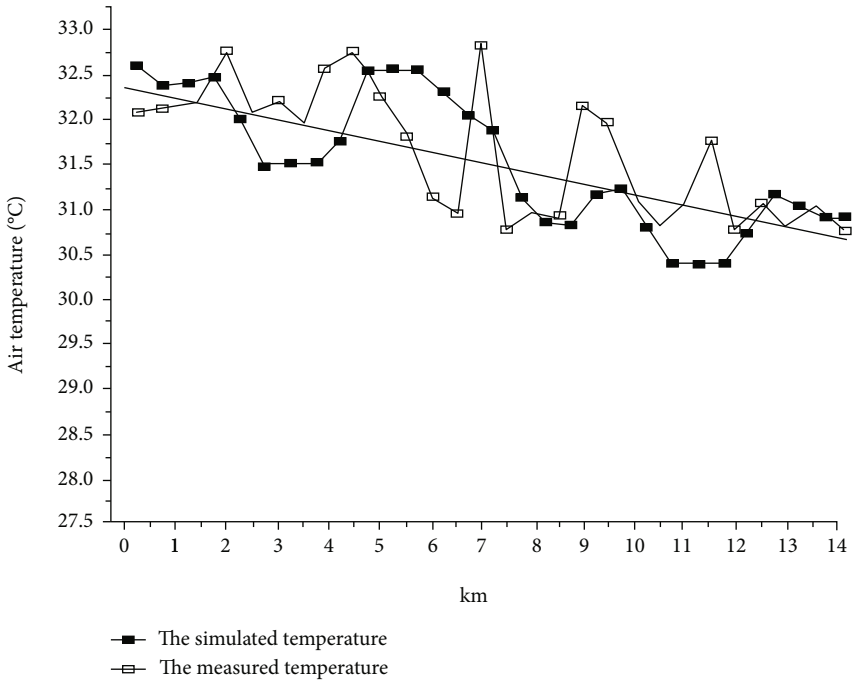

Figure 2: Comparison of simulated and measured results.

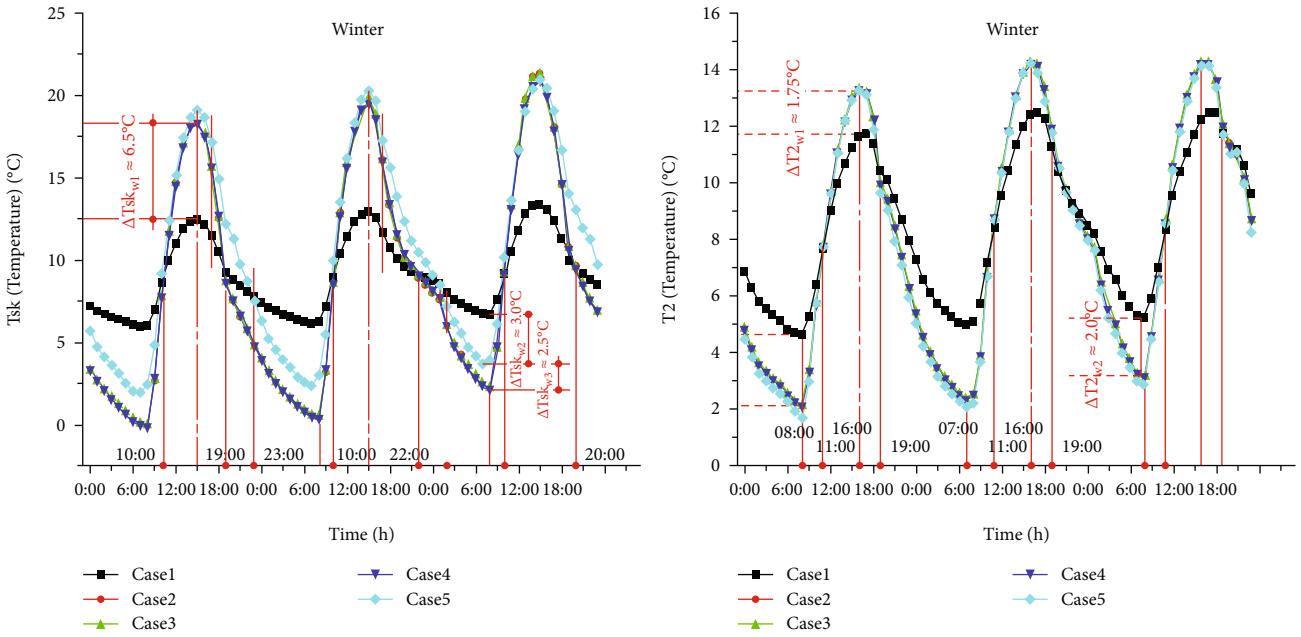

Figure 3: Surface and 2-meter high temperature curve in winter.

simulate the characteristics of urban land types, buildings and ground, multiple long waves between buildings and sky, shortwave reflection process, and other physical processes. The physical scheme selected in this study is shown in Table 1. In the early stage of the experiment, the research team updates the WRF static geographic data. The experiment uses a three-layer nested grid with two-way feedback, the vertical height is 20 km, and the number of interpolation layers is 35. The details of domain 1, domain 2, and domain 3 and the simulation center points are shown in Figure 1 and Table 2. The initial field uses the NCEP/NCAR1° ×1° FNL data of 2017.01.22–2017.01.27 and 2017.07.22–2017.07.27 (world time), and the side boundary is updated every 6 hours.

According to the Wuhan City Master Plan and the Interim Regulations on the Management of Land Use Intensity in the main urban area, as well as the parameter factor variable requirements of the WRF model, we divide the city

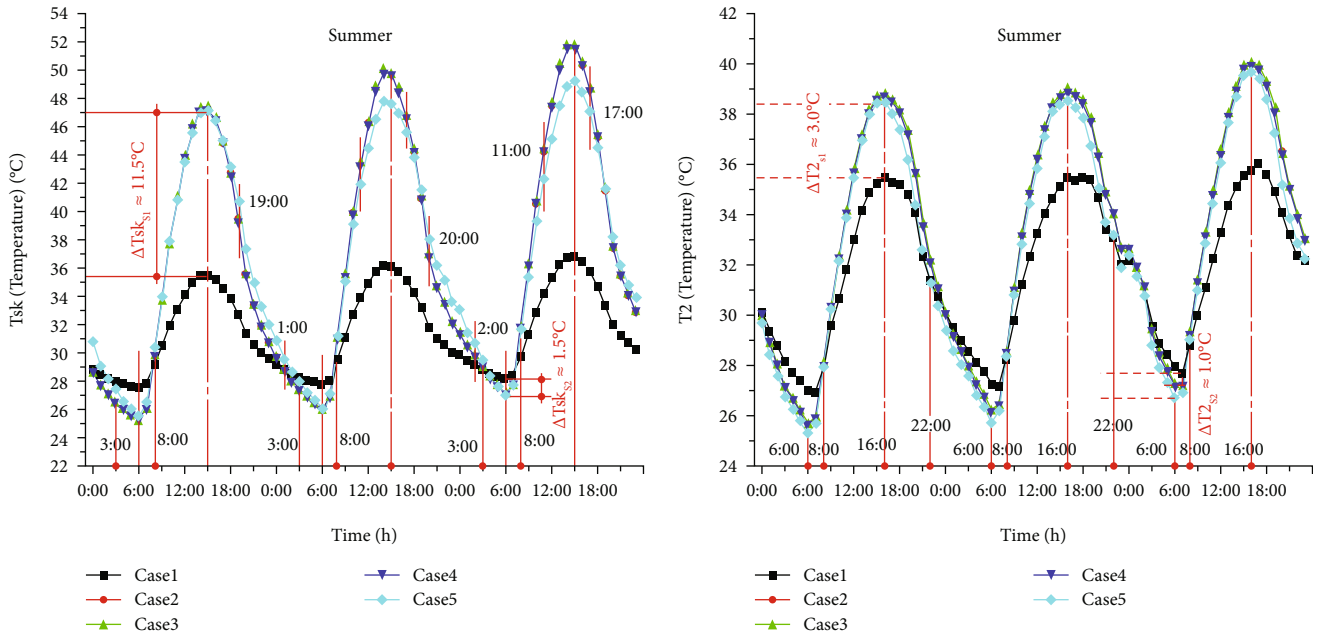

Figure 4: Surface and 2-meter high temperature curve in summer.

into three land use intensity zones. Within the second loop of the city is a high-use intensity zone (H), between the second and third loop lines is a medium-use intensity zone (M), and between the third loop line and the outer loop line is a low-use intensity zone (L) (Figure 1). Table 3 shows the parameter settings of each land intensity zone in the urban canopy model. After comparing the simulated temperature of a certain section of Xiongchu Avenue in Wuhan City with the measured data at a height of 2 meters, the results show a high degree of similarity (Figure 2). Therefore, we believe that the WRF simulation setting based on the urban canopy model (UCM) is accurate and reliable, meeting our requirements.

3. Results and Analysis

3.1. Temperature Curve Analysis. In order to visually display the urban meteorological conditions of ecological patches with different attributes, we only extract the surface temperature Tsk at each case patch in winter and summer and the temperature $T2$ curve at a somatosensory height of 2 meters (Figures 3 and 4) and high temperature field and temperature difference field map within the range of 2 meters in domain 3 (Figure 5, Figure 6).

3.1.1. Comparison of Temperature Curves in Winter. Figure 3 of the winter temperature curve shows that as the sun increases during the day, patches of various attributes have different representations of solar radiation energy. Due to the large specific heat capacity of the water body, the surface temperature is between 10:00 am and 19:00 pm. $\mathrm{Tsk}_{\mathrm{case1}}$ is lower than other cases. Around 15:00, when the surface temperature Tsk of all cases reaches the highest value, the temperature difference between case 1 and others is the most obvious: $\Delta\mathrm{Tsk}_{w1} = \mathrm{Tsk}_{\mathrm{case2/3/4/5}} - \mathrm{Tsk}_{\mathrm{case1}} \geq 6.5°\mathrm{C}$, the temperature of other cases is approximately equal. After 19:00, $\mathrm{Tsk}_{\mathrm{case1}}$ is gradually higher than other cases. At 23:00, $\mathrm{Tsk}_{\mathrm{case1}}$ exceeds all cases until 10:00 the next morning. Tsk of all cases reaches the lowest value at 7:00-8:00 o'clock in the early morning of the next day: $\Delta\mathrm{Tsk}_{w2} = \mathrm{Tsk}_{\mathrm{case1}} - \mathrm{Tsk}_{\mathrm{case5}} \geq 3.0°\mathrm{C}$, $\Delta\mathrm{Tsk}_{w3} = \mathrm{Tsk}_{\mathrm{case5}} - \mathrm{Tsk}_{\mathrm{case2/3/4}} \geq 2.5°\mathrm{C}$. After sunset to 10:00 am the next morning: $\mathrm{Tsk}_{\mathrm{case5}} > \mathrm{Tsk}_{\mathrm{case2/3/4}}$, the surface temperature characterization of the three cases of case 2/3/4 is basic unanimous at all times of the day.

The temperature $T2$ at a height of 2 meters is the body temperature, which is determined by the influence of the surface temperature and the surrounding environment. The temperature reaches its lowest value between 7:00 and 8:00 in the early morning: $\Delta T2_{w2} = T2_{\mathrm{case1}} - T2_{\mathrm{case2/3/4/5}} \geq 2.0°\mathrm{C}$. $T2$ in all cases reaches the highest value at 16:00, which is 1 hour later than the highest value of surface temperature: $\Delta T2_{\mathrm{w1}} = T2_{\mathrm{case2/3/4/5}} - T2_{\mathrm{case1}} \geq 1.75°\mathrm{C}$. It can be seen from the $T2$ curve that the water plaques $T2_{\mathrm{case1}}$ is higher than the value of other cases in the past 17 hours (19:00 to 11:00 the next day), indicating that the water plaques will have positive regulation effect in warming the surrounding areas most of the time.

Comparing the curves of Tsk and $T2$, from 19:00 to 10:00 in the morning of the next day, $T2_{\mathrm{case2/3/4/}}$ is slightly higher than $T2_{\mathrm{case5}}$, and this time period $\mathrm{Tsk}_{\mathrm{case2/3/4}}$ is lower than $\mathrm{Tsk}_{\mathrm{case5}}$. The difference between $\mathrm{Tsk}_{\mathrm{case5}}$ and $T2_{\mathrm{case5}}$ is very small, while the difference between $\mathrm{Tsk}_{\mathrm{case2/3/4}}$ and $T2_{\mathrm{case2/3/4}}$ is more obvious, indicating that the improvement of $T2_{\mathrm{case2/3/4}}$ stems from the role of the surrounding base (construction land). Wuhan is a city with a population of over 10 million. In this case, the index of land use intensity is set according to high standards. If the intensity of buildings around the patch decreases, the man-made heat production decreases, the greening rate increases, the

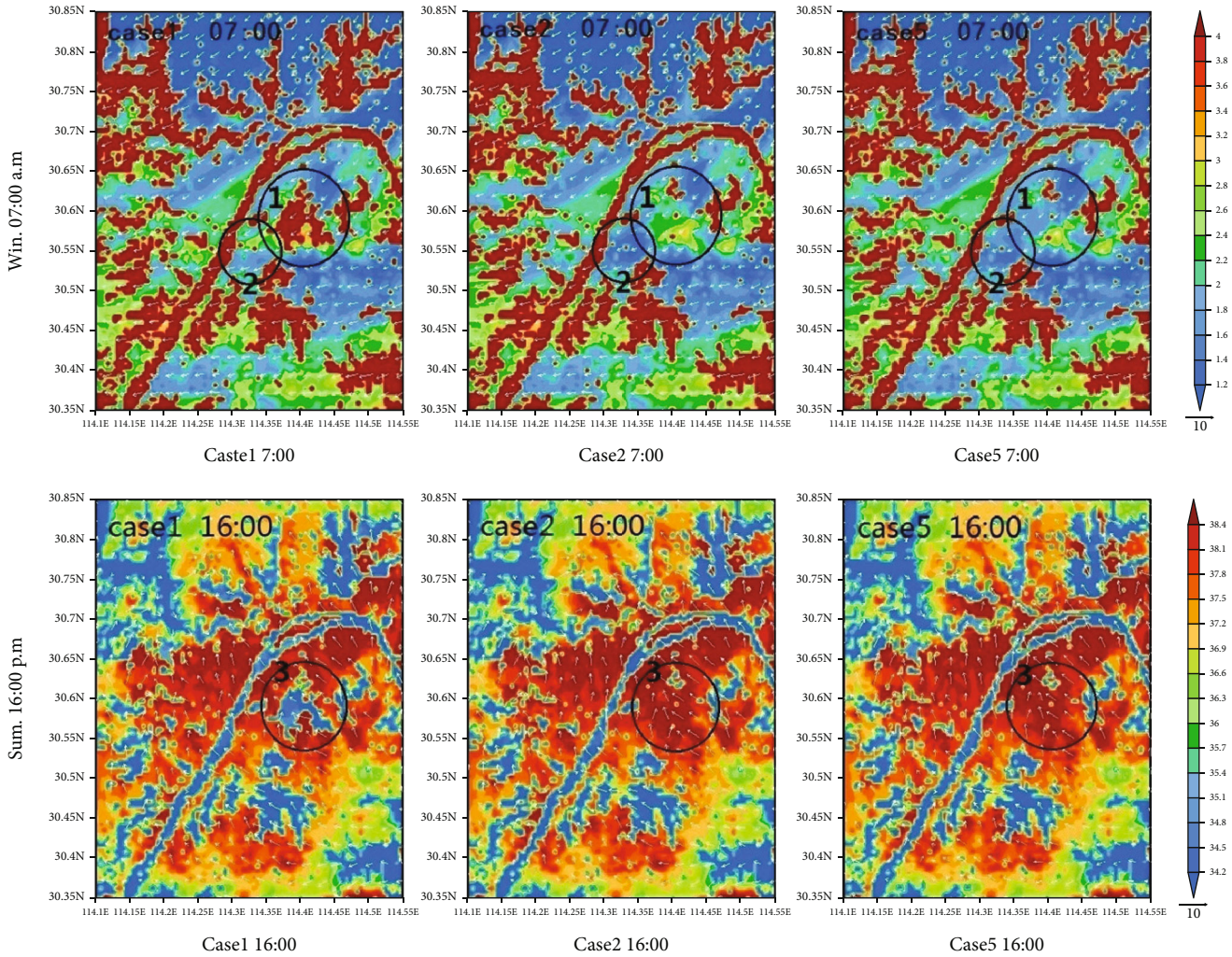

Figure 5: 2-meter high temperature-wind field map in winter and summer.

corresponding energy obtained by the patch will be reduced, and $Tsk_{case2/3/4}$ will be significantly reduced, and as a result, it will affect the periphery of the patch, especially the $T2$ value of the downwind part. The case 2/3/4 patch will have a negative spillover effect on the air temperature in the downwind direction.

3.1.2. Comparison of Summer Temperature Curves. Figure 4 shows that in summer, between 8 : 00 am and 3 : 00 am the next day, Tsk_{case1} is lower than other cases, Tsk reaches the highest value in each case at 14 : 00-15 : 00: $\Delta Tsk_{S1} = Tsk_{case2/3/4/5} - Tsk_{case1} \geq 11.5°C$; the duration is nearly 18 hours, indicating that case 1 can well alleviate the surrounding high temperature for a long time. At 3 : 00-8 : 00 am, Tsk_{case1} is higher than other cases. At 6 : 00 am, Tsk of all cases reaches the lowest value, $\Delta Tsk_{S2} = Tsk_{case1} - Tsk_{case2/3/4/5} \approx 1.5°C$. During the period from 11 : 00 noon to before sunset, the temperature of Tsk_{case5} is relatively low due to the building's obscuration of part of the sun, and the maximum temperature can reach 1-2°C.

The steam temperature curve at a height of 2 meters shows that from 8 : 00 am to 22 : 00 pm, $T2_{case1}$ is lower than other cases; when $T2$ reaches the highest value in all cases at 16 : 00, the temperature difference between case 1 and other cases is the most obvious: $\Delta T2_{S1} = T2_{case2/3/4/5} - T2_{case1} \geq 3.0°C$. From 22 : 00 pm to 8 : 00 am the next day, $T2_{case1}$ is higher than or equal to other cases. When $T2$ reaches the lowest value in all cases at 6 : 00 in the morning, the temperature difference between case 1 and other cases is also obvious: $\Delta T2_{S2} = Tsk_{case1} - Tsk_{case5} \approx 1.0°C$. $T2$ reaches its highest value at 16 : 00-17 : 00. From the analysis of the curve in Figure 4, it can be seen that the case 1 plaque can well relieve the surrounding high temperature for a long time.

3.2. Analysis and Comparison of Temperature-Wind Field and Temperature Difference-Wind Field. In this study, we select the coldest day in winter at 07 : 00 in the morning and the hottest day in summer at 16 : 00 in temperature-wind field (due to the consistent performance of the case 2/3/4 temperature fields, the case 2 temperature-wind field picture represents the picture of case 3/4). At 07 : 00 in the early morning in winter, the northeast wind is the dominant wind direction, light wind is 2-3 m/s, and the temperature is

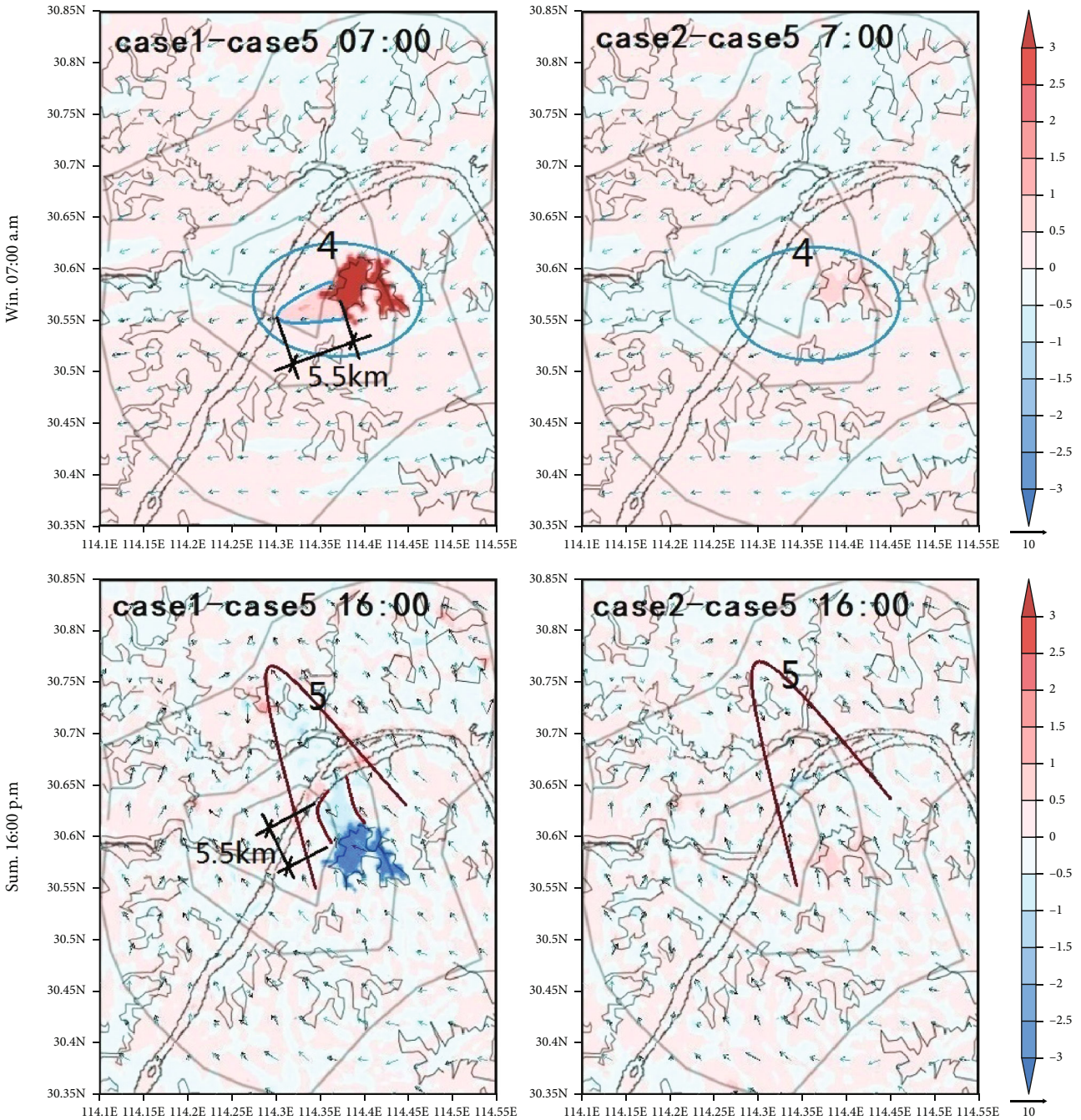

Figure 6: Temperature difference between 2 meters high in winter and summer-wind field map.

the highest at the case 1 patch in each temperature-wind field diagram, which clearly outlines the shape of the east lake water surface, the temperature of case 2/5 patch is obviously lower, and there is no trace of plaque shape (see circle 1 in Figure 5). The air temperature field in the downwind direction of the target patch in case 1 is higher than that in case 2/5 (see circle 2 in Figure 5), indicating that the winter water patches increase the air temperature in the downwind direction, showing the positive spillover effect of temperature adjustment. At 16:00 in the summer, the dominant wind direction is southeast wind, and breeze is 3-4 m/s. For case 1, the temperature at the target patch is the lowest, and the shape of the water surface of the east lake is clearly outlined. The temperature field at the patch 2/5 is the same. At this moment, the climate spillover effect around the patch in the temperature field is not obvious (see circle 3 in Figure 5).

In order to show the spillover effect of the ecological patch temperature more vividly, we select the 2 m high temperature-wind difference field at 07:00 in winter and 16:00 in summer. Figure 6 (due to the consistent performance of the case 2/3/4 temperature field, therefore, the

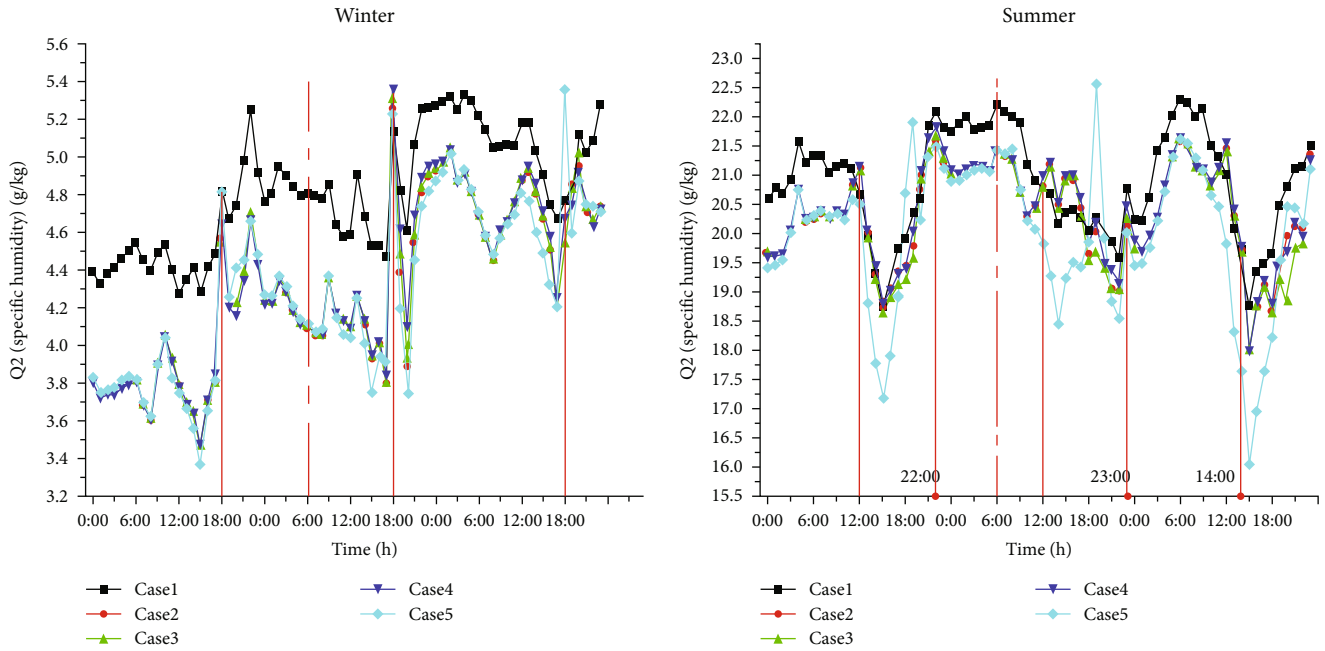

Figure 7: Humidity curve comparison diagram of each case at patch in winter and summer.

temperature difference-wind field in case 2 is a graph representing case 3/4) shows that from 07 : 00 in the early morning, the temperature difference at the target patch during the lowest temperature period in winter (case 1-case 5) is very obvious. There is a red triangle color block in the downwind direction, the temperature difference is 0.5 to 1.0°C, and the distance exceeds 5.5 km. In addition, there are occasional small spots with a temperature difference of 1 to 1.5°C, indicating that the winter water patches have a higher impact on the air temperature in the downwind area than the construction land; that is, the water patches at this moment show a positive spillover effect (Figure 6). The temperature difference field of case 2-case 5, case 3-case 5, and case 4-case 5 is the same, the temperature difference within the patch boundary is within 0.5°C, and the effect on the wind direction down the patch is not obvious (circle 4 in Figure 6). In summer 16 : 00 (case 1-case 5), the temperature difference in the patch is obvious, and there is a temperature difference of 0.5-1°C within a distance of at least 5.5 km in the downwind direction, which has a significant cooling effect. Other difference field diagrams have no obvious spillover effect (see circle 5 in Figure 6).

3.3. Analysis of Wet Environment. Specific humidity is the ratio of the mass of water vapor in a mass of humid air to the total mass of the mass of air (the mass of water vapor plus the mass of dry air). More than 90% of the water vapor in the upper atmosphere of China is concentrated in the middle and lower troposphere, and the specific humidity decreases rapidly with the increase of height. The annual average specific humidity climate field shows a zonal distribution of high in the south and low in the north. Temperature, sea land differences, and atmospheric circulation are the main factors affecting the specific humidity distribution. Regional differences show that the specific humidity rise in the northwest of the middle and lower troposphere is the most obvious, and the rise in the Yangtze River Basin and South China is small. Seasonal differences show that the specific humidity of the lower troposphere tends to increase from 1958 to 2005, mainly in summer and winter. The specific humidity increased in all seasons from 1979 to 2005, and the upward trend in summer is the most obvious. It can be seen from Figure 7 that the specific humidity of the patches in each case is 15 g/kg higher in summer than in winter. In winter, the specific humidity of case 2/3/4/5 is basically the same, and the specific humidity of case 1 is 0.3-0.8 g/kg higher than other cases. In summer, from 0 : 00 to 12 : 00, the specific humidity of case 1 is about 1 g/kg higher than other cases. From 12 : 00 to 18 : 00, the specific humidity of case 5 is lower than other cases. Figure 8 is the field diagram of the specific humidity difference at 6 o'clock in the morning at the representative time of winter and summer (the case 2/3/4 water vapor field is the same, so the case 2 water vapor difference-wind field is represented). There is a significant difference in red water vapor in winter and summer and light red in the downwind direction of the patch, indicating that the water body patch has a higher specific humidity, and the overflow effect causes a slightly higher water vapor ratio in the downwind direction.

And most of the downwind area of the patch (case 2-case 5, case 3-case 5, case 4-case 5) is light blue, indicating that at this moment case 2/3/4 is closer than the wetness compared to the downwind area of the case 5 patch. Summer (case 2-case 5) does not show obvious spillover effects. As Wuhan is an area with wet and cold winters and a higher degree of humidity in summer, although the water patches in the two seasons show the humidification effect (negative

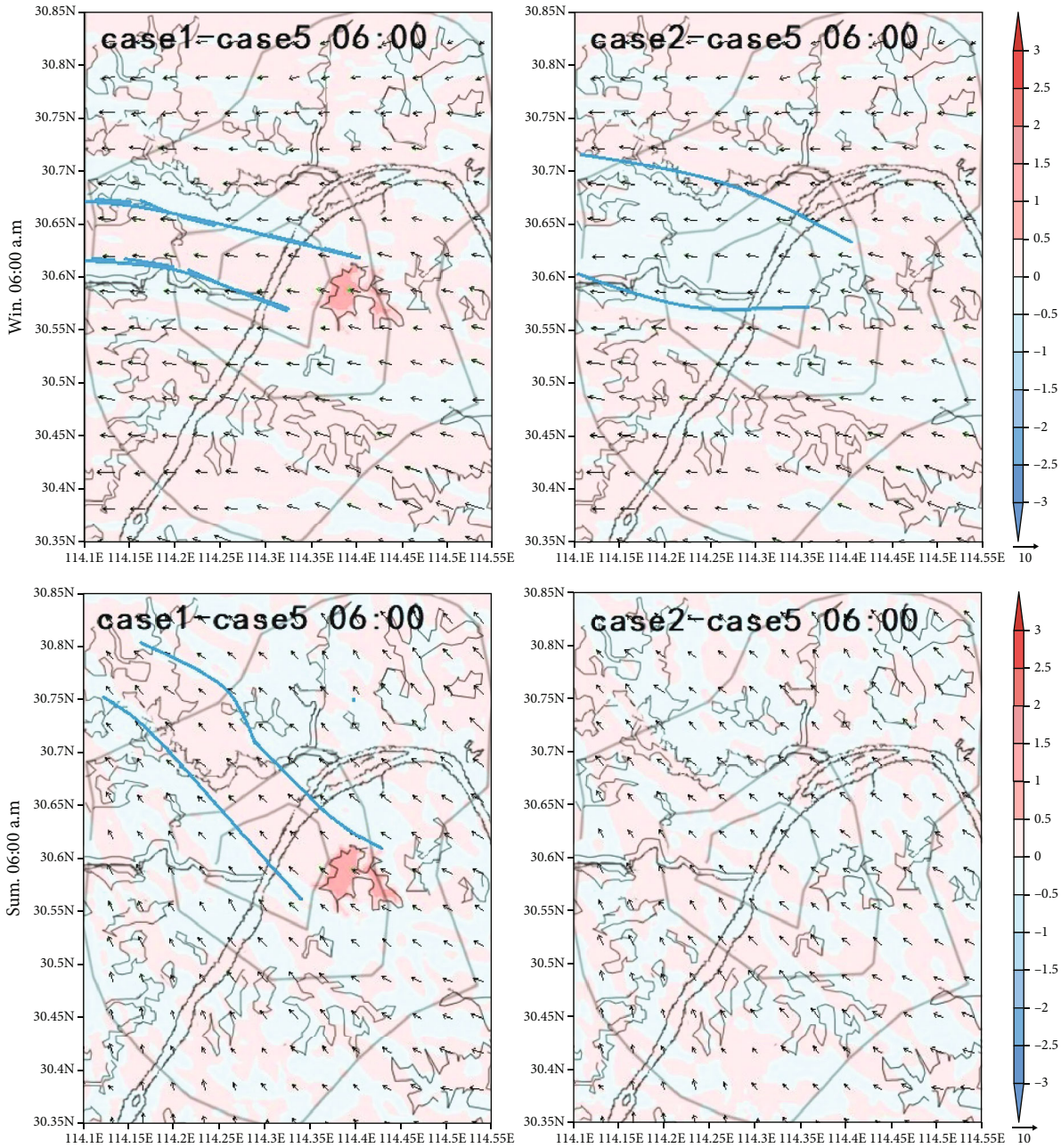

Figure 8: Water vapor difference field diagram at 06 : 00 in the morning in winter and summer.

spillover effect) in the downwind area, but due to the high summer humidity in the hot summer and cold winter area, the humidity will make the human body less comfortable. Vegetation/arable land, wetland, and woodland patches show weak positive spillover effects in the downwind direction in winter.

4. Conclusion

(1) Water patches show a positive spillover effect on their downwind parts from sunset in winter to the morning of the next day and in summer from 8 : 00 a.m. to 22 : 00 pm, improving the temperature conditions of this part to varying degrees. The highest surface temperature difference between water patches and patches with other attributes ΔTsk is up to 6.5°C in winter and 11.5°C in summer. The highest temperature difference at a somatosensory height of 2 meters $\Delta T2$ is up to 2.0°C in winter and 3.0°C in summer, which can significantly improve the surrounding environment. During the coldest period in winter and the hottest period in summer, under light wind conditions, patches of water will have a positive spillover effect within 5.5 km of the downwind direction. Based on the above analysis of temperature and humidity environment and

consideration of climate regulation, the best distribution of water patches is in the north or northeast of the city, followed by the south or southwest

(2) The sensory temperature at a height of 2 meters is not entirely determined by the surface temperature. When it is affected by the surrounding environment, it may not be consistent with the surface temperature. Therefore, the accuracy of the method of studying the temperature in the urban canopy through surface images is very important

(3) In winter, from 19 : 00 am to 10 : 00 am the next day, if the intensity value of the construction land around the patch is lower than the value set in this study (based on the development of the city, this setting takes a higher value), vegetation/arable land, wetland, and woodland patches will have a negative spillover effect on the air temperature in the downwind direction. Therefore, the vegetation/arable land and wetland patches can be appropriately reduced in the northern and northeastern parts of the city

Data Availability

The figures and tables used to support the findings of this study are included in the article.

Conflicts of Interest

The authors declare that they have no conflicts of interest.

Acknowledgments

This work was supported by projects of the National Natural Science Foundation of China (Project No. 51778251), the Hubei Meteorological Bureau Science and Technology Development Foundation of China (Project No. 2018Z10), and the 2020 College Student Innovation and Entrepreneurship Program of China (Project No. X202010500115).

References

[1] Y. Tian and C. Y. Jim, "Factors influencing the spatial pattern of sky gardens in the compact city of Hong Kong," *Landscape and Urban Planning*, vol. 101, no. 4, pp. 299–309, 2011.

[2] Z. Y. Sun, T. Ma, J. Ma, R. Ma, and C. M. Yan, "Effect of strata heterogeneity on spatial pattern of land subsidence in Taiyuan City," *Rock and Soil Mechanics*, vol. 28, no. 2, pp. 399–403, 2007.

[3] K. L. Chen, J. Z. Gong, and X. Y. Chen, "Spatial pattern and differentiation characteristics of urban heat island intensity in Guangzhou city," *Chinese Journal of Ecology*, vol. 36, no. 3, pp. 792–799, 2017.

[4] Y. Hori, M. Shiyomi, S. I. Aikawa, H. Ogitsu, and T. Yasuda, "Spatial pattern differences in land use between mountainous, agricultural and city districts in Ibaraki prefecture, Japan," *Japanese Journal of Ecology*, vol. 55, no. 1, pp. 11–19, 2005.

[5] H. Chen, D. Zhu, W. Yun, L. Yang, and C. Tang, "Analysis on cultivated land fragmentation and spatial agglomeration pattern in Jiaxing city," *Transactions of the Chinese Society of Agricultural Engineering*, vol. 28, no. 4, pp. 235–242, 2012.

[6] G. Tian, J. Wu, and Z. Yang, "Spatial pattern of urban functions in the Beijing metropolitan region," *Habitat International*, vol. 34, no. 2, pp. 249–255, 2010.

[7] G. Jin, X. Shi, D. He, B. Guo, and X. Shi, "Designing a spatial pattern to rebalance the orientation of development and protection in Wuhan," *Journal of Geographical Sciences*, vol. 30, no. 4, pp. 569–582, 2020.

[8] J. J. Li, X. R. Wang, X. J. Wang, W. C. Ma, and Z. Hao, "Remote sensing evaluation of urban heat island and its spatial pattern of the Shanghai metropolitan area, China," *Ecological Complexity*, vol. 6, no. 4, pp. 413–420, 2009.

[9] Z. Q. Xie, Y. Du, Y. Zeng, M. L. Yan, and C. Y. Zhu, "Accelerated human activities affecting the spatial pattern of temperature in the Yangtze River Delta," *Quaternary International*, vol. 226, no. 1-2, pp. 112–121, 2010.

[10] Y. B. Wang, C. W. Liu, P. Y. Liao, and J. J. Lee, "Spatial pattern assessment of river water quality: implications of reducing the number of monitoring stations and chemical parameters," *Environmental Monitoring and Assessment*, vol. 186, no. 3, pp. 1781–1792, 2014.

[11] Z. Ning, W. Cheng, H. Zhou, and L. Min, "Analysis on instantaneous spatial pattern of thermal force field in Harbin," *Chinese Journal of Applied Ecology*, vol. 14, no. 11, pp. 1955–1958, 2003.

[12] B. Thompson, N. Dunse, C. Jones, J. Brown, and W. D. Fraser, "The spatial pattern of industrial rents and the role of distance," *Journal of Property Investment & Finance*, vol. 23, no. 4, pp. 329–341, 1999.

[13] W. Ding and Z. Tong, "An approach for simulating the street spatial patterns," *Building Simulation*, vol. 4, no. 4, pp. 321–333, 2011.

[14] N. Mou, C. Wang, J. Chen, T. Yang, L. Zhang, and M. Liao, "Spatial pattern of location advantages of ports along the Maritime Silk Road," *Journal of Geographical Sciences*, vol. 31, no. 1, pp. 149–176, 2021.

[15] Y. Jing, Q. Xie, and N. Tan, "National land spatial pattern distribution method based on ecological carrying capacity," *Transactions of the Chinese Society of Agricultural Engineering*, vol. 33, no. 11, pp. 262–271, 2017.

[16] G. Jiang, X. He, W. Ma, M. Wang, and R. Zhang, "Rural settlements spatial pattern evolution and zoning district based on spatial autocorrelation," *Transactions of the Chinese Society of Agricultural Engineering*, vol. 31, no. 13, pp. 265–273, 2015.

[17] W. Yue, L. Yong, P. Fan, X. Ye, and C. Wu, "Assessing spatial pattern of urban thermal environment in Shanghai, China," *Stochastic Environmental Research and Risk Assessment*, vol. 26, no. 7, pp. 899–911, 2012.

[18] C. Y. Jim and W. Y. Chen, "Diversity and distribution of landscape trees in the compact Asian city of Taipei," *Applied Geography*, vol. 29, no. 4, pp. 577–587, 2009.

[19] B. Ermentrout and M. Lewis, "Pattern formation in systems with one spatially distributed species," *Bulletin of Mathematical Biology*, vol. 59, no. 3, pp. 533–549, 1997.